Bipolaronic insulator on alkali/Si(111):B-2$\sqrt{3}$x2$\sqrt{3}$R30° interfaces

Cédric Tournier-Colletta, Luis Alfonso Cardenas Arellano, Yannick Fagot-Revurat, Bertrand Kierren, Antonio Tejeda, Daniel Malterre, Patrick Le Fèvre, François Bertran, Amina Taleb-Ibrahimi

Bipolaronic insulator on alkali/Si(111):B-$2\sqrt{3}\times 2\sqrt{3}R30°$ interfaces

C. Tournier-Colletta,[1,*] L. Cardenas,[1] Y. Fagot-Revurat,[1] B. Kierren,[1] A. Tejeda,[1,2] D. Malterre,[1] P. Le Fèvre,[2] F. Bertran,[2] and A. Taleb-Ibrahimi[2]

[1]*Institut Jean Lamour, UMR 7198, Nancy Université/CNRS, BP 239, F-54506 Vandoeuvre-lès-Nancy, France*

[2]*Cassiopée Beamline, Synchrotron Soleil, BP 48, F-91192 Gif-Sur-Yvette, France*

(Received 29 July 2010; published 15 October 2010)

In this paper, we present a systematic study of the structural and electronic properties of the alkali/Si(111):B interface, combining low-energy electron diffraction and (angle-resolved) photoemission spectroscopy. We show that potassium (K), rubidium (Rb), and caesium (Cs) ultrathin films, including solid solutions K-Rb, share the same physics. First of all, the $2\sqrt{3}\times 2\sqrt{3}R30°$ surface reconstruction, evidenced only very recently using potassium is shown to be a common feature at the saturation coverage. A 3×3 reconstruction is also observed for coverages just below saturation. From an electronic point of view, the band features found with K are generalized. As a distinct point, we evidence that the surface state is constituted by two subbands which have the reconstruction symmetry. At low temperature (55 K), a systematic shift of the surface state toward higher binding energies is observed together with a reduction of its linewidth. A close inspection of the data reveals fine, systematic effects depending on the alkali. Indeed as substituting from K to Cs, the surface-state binding energy is reduced continuously whereas the bandwidth increases. K differs from Rb and Cs, by a smaller reduction of the linewidth and a higher energy shift upon cooling. These features are interpreted consistently within the bipolaron model, which was invoked previously to explain the insulating nature of the K/Si:B surface state. Polaronic effects are shown to be enhanced with K, as already demonstrated on alkali/GaAs(110) interfaces.

DOI: 10.1103/PhysRevB.82.165429 PACS number(s): 73.20.At, 73.22.Gk, 73.20.Mf, 73.22.Dj

I. INTRODUCTION

Semiconductor surfaces have generally a lower symmetry than the bulk termination which is obtained when separating an infinite crystal in two pieces. This is the well-known *surface reconstruction* phenomenon.[1] Basically, it originates from the presence of broken bonds, the so-called *dangling bonds*, localized on the surface adatoms. Thanks to a lattice distortion, different new bonding states are created and then a large portion of the lost binding energy can be regained. Such a situation is found, for example, on the Si(111):B surface.[2] Boron segregation from the bulk induces the $\sqrt{3}\times\sqrt{3}R30°$ hexagonal pattern (thereafter $\sqrt{3}$). Dangling-bond states on the $\sqrt{3}$ geometry have been receiving a lot of interest since it was predicted that they could exhibit important correlation effects.[3,4] The bandwidth of such states is indeed smaller than in the bulk and as a consequence, the criterion $U/W\gtrsim 1$ for the Mott metal-to-insulator transition[5–8] can be fulfilled. An important requirement is the half filling of the dangling bonds; on the clean Si(111):B surface, however, the latter are completely empty. To observe correlation effects, one must provide electrons by depositing metallic atoms, for example. This was achieved using K and Cs.[9–14] At saturation coverage, angle-resolved photoemission spectroscopy (ARPES) does not indicate any sign of metallicity, but an almost flat, insulating surface state.[11–13] Weitering *et al.* proposed this was the signature of the Mott insulating ground state.[12,15,16]

Afterwards, other intriguing, "strongly correlated" $\sqrt{3}$—interfaces have been discovered and are still subject of an intense experimental and theoretical work [$\frac{1}{3}$ monolayer (ML) (Sn,Pb)/Ge(111),[17–25] $\frac{1}{3}$ ML Sn/Si(111),[21,23,26–28] and $\frac{1}{3}$ ML Si/SiC(0001) (Refs. 29–32)]. Similar to (K,Cs)/Si:B, Si/SiC exhibits *at room temperature* an occupied[29,32] and an unoccupied[30,32] surface state, which are very weakly dispersive and separated by a large gap ($\approx$2 eV); likely, they correspond to the *U*-splitted Hubbard bands, resulting from the Mott transition.[31] Sn/Ge owns a richer phase diagram as a function of temperature. At room temperature, the interface is characterized by a metallic surface state.[19] At $\approx$200 K, a first transition from the $\sqrt{3}\times\sqrt{3}R30°$ to the 3×3 reconstruction occurs[18] while surface band structure remains almost identical;[19] an order-disorder mechanism involving the dynamical fluctuations of Sn adatoms[20,25] is now accepted. Finally at very low temperature ($\approx$20 K), a second transition stabilizes the $\sqrt{3}$ together with the opening of an energy gap ($\approx$0.8 eV);[22] here again, the Mott insulating ground state has been invoked. In the case of Sn/Si, the Mott state is reached at $\approx$70 K,[23,28] but no 3×3 has been observed at intermediate temperatures.[26,28]

In addition to strong correlations, polaronic effects due to strong electron-phonon (e-ph) interaction may be important. A relevant indication is given by the inspection of the ARPES line shape, which is basically related to the one-hole spectral function.[33] Very broad spectral structures may be the signature of such a strong coupling. This is the so-called "Frank-Condon" broadening, which originates from the cloud of virtual phonons forming around the electrons.[34] In some cases, for example, alkali/GaAs(110),[35,36] polaronic effects are so strong that they overwhelm the electronic repulsion. Associated with a lattice distortion, localized electron pairs—the *bipolarons*—form. On the half-filled atomic chain, a doubling of the unit cell occurs, the system consisting in an alternance of empty and doubly (the bipolaron) occupied atomic sites; this is the so-called *bipolaronic insulator* ground state.[37,38] Recently, the $2\sqrt{3}\times 2\sqrt{3}R30°$ recon-

struction, $2\sqrt{3}$ for short, has been observed on K/Si(111):B.[14] This doubling of the unit cell, in the two surface directions, favors a two-dimensional bipolaronic insulator ground state instead of the Mott state. Now the question arises whether this behavior is specific to K or generic to all alkali/Si:B interfaces. We present therefore a systematic study with different alkali species (K, Rb, Cs, and K-Rb solid solution), combining low-energy electron diffraction (LEED) and photoemission spectroscopy. The paper is organized in two sections. In the first one, we check the surface structure symmetry as a function of alkali coverage. The $2\sqrt{3}$ is observed systematically at room temperature; a new feature is the 3×3 reconstruction forming below saturation coverage. In the second section, we examine the surface electronic band structure using ARPES. The main features found with K are generalized; as a new point, we evidence that two subbands having the lattice symmetry constitute the surface state. Finally, the ARPES line shape is analyzed in detail; we observe fine temperature effects depending on the alkali, which are interpreted within the bipolaron model.

II. EXPERIMENT

The experiments have been performed in a ultrahigh vacuum set up which couples a preparation chamber equipped with LEED and Auger spectroscopy and a high-resolution ARPES chamber. The substrate is a highly boron-enriched Si(111) sample, Si:B for short ($\rho \approx 10^{-3}$ Ω cm). For such doping concentration, silicon turns out to be a degenerate semiconductor[39] with bulk *sp* bands crossing the Fermi energy.[40,41] After a long outgassing by direct resistive heating, the sample is progressively flashed up to 1500 K. During this step, pressure never exceeds 2×10^{-9} mbar. Then follows a long annealing at 1100 K which makes boron atoms segregate to the surface. This procedure leads to the $\sqrt{3}$ hexagonal surface reconstruction, as checked by LEED. Alkali atoms—potassium (K), rubidium (Rb), and caesium (Cs)—are provided by commercial getters from the SAES firm; these are based on the thermally activated reduction of an alkali chromate. The getters have been carefully outgassed so that the pressure keeps in the low 10^{-10} mbar (H_2 mainly) during evaporation. The typical flow is 0.1 ML per minute, where 1 ML stands for 1 atom per each 1×1 unit cell. When evaporating on a room-temperature substrate, alkali dosis saturates at the surface. The design of the evaporation chamber allows to evaporate simultaneously two alkali metals. Angle-resolved photoemission measurements are carried out with a Scienta SES 200 analyzer. The photon source is a Specs helium discharge lamp, which is monochromatized on the He I ($h\nu$=21.21 eV) energy. Alkali-covered surfaces are subject to a quick contamination (the surface state is killed after 30 min exposure to the UV beam), so we perform ARPES measurements with pass energy 10 eV and 0.5 mm—width slits in order to have sufficient signal/noise ratio for relatively short acquisition times (typically, 10 min for the intensity maps presented in this paper). Under these conditions, the energy and angle resolutions are 10 meV and 0.2°, respectively. Fermi energy is measured on a molybdenum part on the sample holder. Complementary to valence-band measurements, core-levels photoemission provided by a x-ray source (Mg, $h\nu$=1253.6 eV) allows the chemical analysis of the interfaces. Additional photoemission measurements, including polarized-light band structure and high-resolution core levels,[42] have been performed on the Cassiopée beamline at Synchrotron Soleil.[43,44]

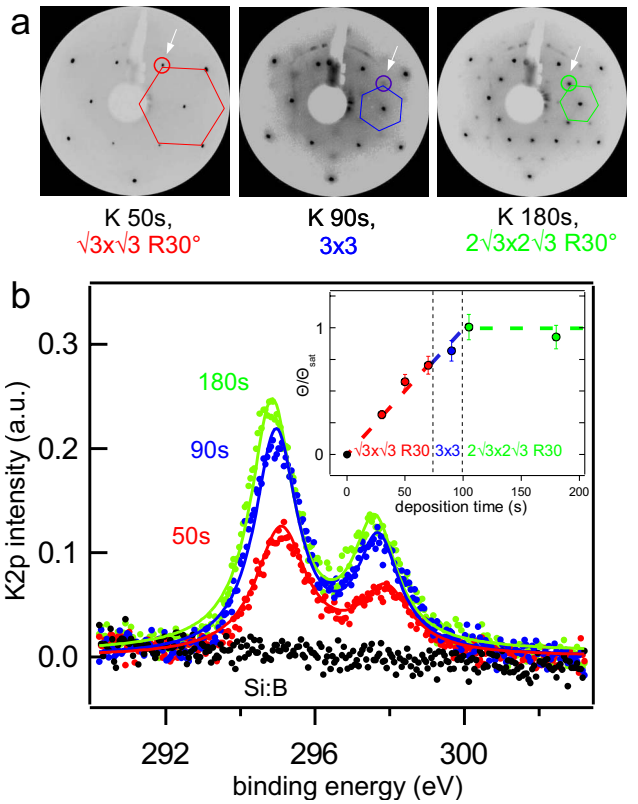

FIG. 1. (Color online) (a) Leed patterns taken at E=45 eV for increasing potassium deposition at room temperature; the arrows indicate the additional spots due to the surface reconstruction. (b) Corresponding XPS K 2*p* spectra recorded at room temperature (points); the plain lines are the Lorentzian fits, the integrated area of which are proportional to the K coverage. Inset: structural phase diagram as a function of K coverage.

III. STRUCTURE OF THE ALKALI/SI:B INTERFACES

A. LEED and XPS results

It has been discovered only very recently[14] that the deposition of potassium, at room temperature, on the Si:B substrate leads to the $2\sqrt{3}$ surface reconstruction at saturation coverage. Since former studies on this system, saturation coverage is supposed to correspond to one potassium atom per $\sqrt{3}$ unit cell;[15,16] nevertheless we stress that this assumption has not yet been demonstrated experimentally. By combining LEED [Fig. 1(a)] and x-ray photoemission spectroscopy (XPS) [Fig. 1(b)], we have explored lower coverages in order to understand the growth of this interface and the existence of this new reconstruction. Alkali coverage is extracted as follows: we have subtracted a Shirley background from the XPS spectra and fitted the resulting with two Lorentzian functions which reproduce the 2*p* spin-orbit split-

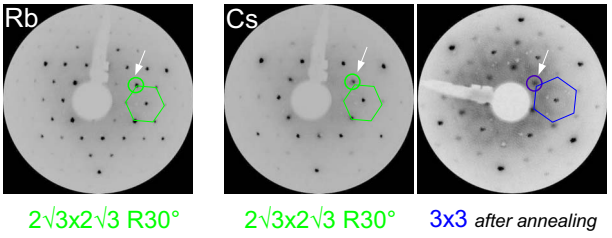

FIG. 2. (Color online) LEED patterns taken at $E=40$ eV for Rb and Cs/Si:B interfaces at saturation coverage. As for K, the surface is $2\sqrt{3}$—reconstructed. After a short annealing at 500 K, the $2\sqrt{3}$ is destroyed at the benefit of the 3×3 reconstruction, as shown in the right picture for a Cs interface.

ting; then the integrated area of the fit is directly proportional to the number of surface potassium atoms. In the "low" coverage regime, i.e., less than 75% of the saturation coverage, the interface preserves the $\sqrt{3}$ symmetry of the substrate. For deposition times greater than 100 s, the integrated area of the K $2p$ XPS line keeps constant showing that the amount of potassium saturates at the surface. In this case, the $2\sqrt{3}$ reconstruction takes place as in the previous experiments.[14] An interesting point comes from the intermediate coverages, roughly between 75% and 100% of the saturation coverage. In this range, the $2\sqrt{3}$ is generally not observed so we conclude that this reconstruction is stable only at the saturation coverage; still we observe a distinct ordered phase, namely, the 3×3 reconstruction. The structural phase diagram is shown in the inset, Fig. 1(b). The 3×3 can be destroyed easily at the benefit of the $2\sqrt{3}$ by further potassium deposition. Reciprocally, the $2\sqrt{3}$ can be destroyed at the benefit of the 3×3 by a few minutes annealing at 500 K which removes a small fraction of potassium. Finally, the two patterns are sometimes found to coexist. This set of observations suggests a subtle competition between these two phases as a function of coverage.

Then we have extended the study to the two alkali materials which follow potassium in the first column of the periodic table, namely, rubidium (Rb) and caesium (Cs) to check if the $2\sqrt{3}$ reconstruction is a generic property of alkali/Si:B interfaces. For example, a systematic behavior has been already observed for alkali deposited on the Si(111) 7×7 surface, which reconstructs into the 3×1 at $\frac{1}{3}$ ML coverage (for a review, see Ref. 45). As shown in Fig. 2, the $2\sqrt{3}$ reconstruction is recovered on saturated Rb and Cs/Si:B interfaces. The 3×3 is recovered also by slightly annealing a saturated interface at moderate temperature (500 K), for example, Cs/Si:B in the figure. One step further is carried out by coevaporating two different alkali's (Fig. 3). We have evaporated simultaneously K and Rb during a time that corresponds to the saturation coverage of a single alkali species; however, the *total* amount of alkali at the surface still corresponds to that of a pure saturated interface. In Fig. 3(b), comparison of the K $2p$ and Rb $3p$ XPS lines (green plain lines) with those recorded on the respective pure interfaces (red dashed lines) gives a saturated interface which composition is 40% K and 60% Rb. As for the pure interfaces, we observe the $2\sqrt{3}$ reconstruction [Fig. 3(a)]. To check the quality of the crystallographic order, the width of a $2\sqrt{3}$ LEED spot is compared to that on the pure Rb interface. The width is nearly identical so the coherence length—the size of the $2\sqrt{3}$ domains—remains unaffected. Then the interface is likely to be a homogeneous solid solution.

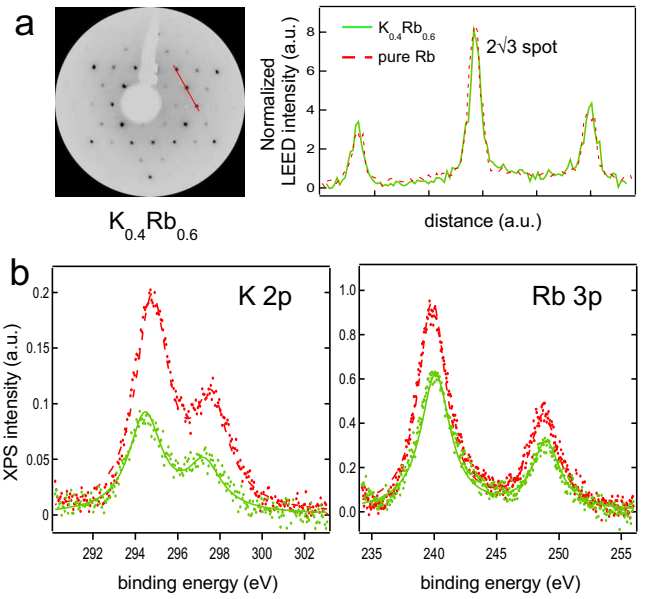

FIG. 3. (Color online) (a) LEED pattern taken at $E=45$ eV on a $K_{0.4}Rb_{0.6}$/Si:B-$2\sqrt{3}$ solid solution. (b) Corresponding XPS K $2p$ and Rb $3p$ lines: the green plain line is for the K-Rb solid solution; the red dashed lines are for pure K and Rb interfaces at saturation coverage.

B. Discussion

In the following, we compare alkali/Si:B to similar systems which exhibit also a $2\sqrt{3}$ or a 3×3 reconstruction, namely, Si/SiC(0001), Sn/Si(111), and Sn/Ge(111). At room temperature, these three interfaces are $\sqrt{3}$ reconstructed for a 1/3 ML coverage (see references in Sec. I). In the case of Si/SiC (Ref. 46) and Sn/Si,[47,48] a $2\sqrt{3}$ phase appears when slightly increasing the adsorbate amount. Such a behavior is not observed in Sn/Ge(111) up to 1/2 ML.[25] However, a 3×3 reconstruction is observed at low temperature (200 K). To summarize, the $2\sqrt{3}$ never forms at 1/3 ML on the similar systems; depending on temperature, the common reconstruction is either the $\sqrt{3}$ or the 3×3. This questions about the absolute coverage for alkali/Si:B. Its knowledge remains a key question, since the ground state depends crucially on the number of electrons transferred to the dangling bonds. For that, we have carried out a comparative study[42] by means of LEED, STM, and XPS with a system whose absolute coverage has been determined experimentally and is widely accepted: K/Si(111) 3×1, whose absolute coverage is 1/3 ML at saturation.[45] Our conclusion is that the coverage corresponding to the $2\sqrt{3}$ is not 1/3 ML but 1/2 ML ($\pm10\%$), that is six alkali atoms per $2\sqrt{3}$ unit cell. This result is thus consistent with what observed on Si/SiC and Sn/Si. According to our XPS calibration (Fig. 1), the 1/3 ML coverage could correspond to the 3×3.

With this new element, we can now discuss the following puzzling point: why previous studies did not evidence the $2\sqrt{3}$ reconstruction? We propose this discrepancy may originate from *different experimental saturation coverages* and point out two possible reasons for that. The first one could be the different ways of detecting alkali saturation: in previous studies,[9–13] it was done mainly by monitoring the *work function* saturation whereas in our case, it is done with *core-levels* saturation. It is possible that the two procedures do not coincide; indeed, it is known that the work function can saturate before the core levels.[1] However, we discard this hypothesis because Weitering *et al.* mention[12] that the work function and the alkali core-level saturate at the same deposition time in their experiments. The second, more likely reason is that the saturation coverage depends on the sample preparation. Specifically, the concentration of boron vacancies,[2] which are very reactive because of their dangling electrons, can be an important factor. The Si:B-$\sqrt{3}$ surface is obtained either by decomposition of decaborane ($B_{10}H_{14}$) (Ref. 12) or, as in our case, by annealing a highly doped substrate; we believe the second procedure produces a surface with much less boron vacancies, and then a higher alkali saturation coverage. Consequently, *it is possible that the saturation coverage was below* 1/2 ML *in the previous studies*. The substrate temperature when evaporating the alkali's is also determining. After outgassing the sample, it may take a long time for the substrate to cool down; actually, it may not be at room temperature during evaporation, leading to the desorption of a fraction of the alkali's.

There is an alternative explanation, which assumes the same 1/2 ML coverage in all experiments: the dependence of the $2\sqrt{3}$ stabilization temperature as a function of the concentration of defects. For instance, in charge-density-wave (CDW) compounds, in which a lattice distortion is involved, it is well known that defects destroy long-range order and lower the transition temperature.[49–51] In the present experiment, the $2\sqrt{3}$ is always observed at room temperature. In the previous study of Cardenas *et al.*,[14] however, the $2\sqrt{3}$ was observed below 270 K; this could be the fact of a higher concentration of defects. Therefore it is not excluded that previous workers would have found the $2\sqrt{3}$ if they had cooled down the sample.

IV. ELECTRONIC PROPERTIES OF THE ALKALI/Si:B-$2\sqrt{3}$ INTERFACES

A. ARPES results

In the case of K and Cs, literature[11–15] states that the main feature observed with ARPES is the appearance of one insulating (fully occupied) *surface* state with 0.6–0.7 eV binding energy and showing weak dispersion (the bandwidth is about 0.2 eV). This state has been shown to derive from sp_z dangling orbitals; the latter are empty on the Si:B $\sqrt{3}$ substrate, then filled by alkali's *ns* electrons upon deposition. In addition, it was emphasized the important energy broadening of the ARPES line and polaronic effects were invoked to explain this observation.[15] Note that no $2\sqrt{3}$ reconstruction was observed during these photoemission measurements (see the discussion, Sec. II). Together with the $2\sqrt{3}$, Cardenas *et al.*[14] evidenced an extremum of the surface-state band at the edge of the $2\sqrt{3}$ Brillouin zone, which was interpreted as the surface reconstruction signature on electronic properties.

Our purpose, here, is to extend the high-resolution surface band-structure measurements to other alkali materials, in order to compare with accuracy the binding energies, bandwidths, and linewidths. In principle, this would give further insight about the polaronic effects, since the latter depend on the polarizability and mass of the atoms.[52] Measurements have been performed on alkali interfaces at saturation coverage only, both at low (55 K) and room temperatures. The corresponding crystallographic structure was always the $2\sqrt{3}$ phase. In Fig. 4, we present new data concerning the pure Rb and Cs/Si:B-$2\sqrt{3}$ interfaces, taken at 55 K. $I(E,\theta)$ intensity maps taken along the $\bar{\Gamma}\bar{K}$ and $\bar{\Gamma}\bar{M}$ directions are given on top of each panel. With a lattice parameter[2] $a=6.65$ Å, $\bar{M}$ and $\bar{K}$ points correspond to 15.5° and 17.5° emission angles, respectively. First as expected, the fully occupied surface-state observed with K (Refs. 14 and 53) is recovered on the Rb and Cs interfaces, in the [−1.0 eV; −0.4 eV] energy range. Superimposed on it and much more dispersive, an extra state arises in the $\bar{\Gamma}\bar{M}$ direction; it is indicated by the brown dotted line. Actually, this state is not induced by alkali deposition but it is one of the substrate bulk states. The yellow points constitute the dispersion of the surface state; they are obtained from a procedure which tracks, for each angle emission, the energy of the intensity maximum. At first glance, we can note that for both Rb and Cs interfaces the amplitude of the dispersion is weaker in the $\bar{\Gamma}\bar{M}$ direction than in the $\bar{\Gamma}\bar{K}$ direction. This is actually a generic feature of bands on the triangular lattice. For Rb, corresponding energy-dispersion curves (EDCs) are plotted below the intensity maps with emphasized high-symmetry points (thick lines). For Cs, two-band mappings taken at different binding energies are presented. At 0.62 eV, the surface state corresponds to the bright pocket at the center whereas the bulk state corresponds to the six crescents around; at 0.4 eV, the tail of the surface state is the only observed spectral feature, forming a hexagonal ring which lies at the edge of the $2\sqrt{3}$ Brillouin zone. Polarized-light measurements (horizontal and vertical polarizations, see scheme) confirm that the Cs surface state has the sp_z symmetry, as in the case of K.[12]

An important point to discuss is the surface-state *symmetry*. For both interfaces and both high-symmetry directions the surface-state clearly exhibits an extremum at the edge of the $2\sqrt{3}$ Brillouin zone, as indicated by the white dotted lines. This result is consistent with previous results on K interfaces:[14,53] in these papers, it is argued this is the signature of the $2\sqrt{3}$ surface reconstruction on the surface electronic structure. An inspection of the Brillouin zones (see scheme on the Cs band mappings, Fig. 4) shows that the $\bar{K}_{2\sqrt{3}}$ and $\bar{K}_{\sqrt{3}}$ points correspond to opposite $\vec{k}$ vectors in the first Brillouin zone. Thus a band having the $2\sqrt{3}$ symmetry *must* have the same energy at these two points. This is clearly not the case if we interpret the data within a single band. In addition when a reconstruction takes place, new bands must arise from the diffusion of the unperturbated states by the Fourier components of the reconstruction potential (*umklapp*

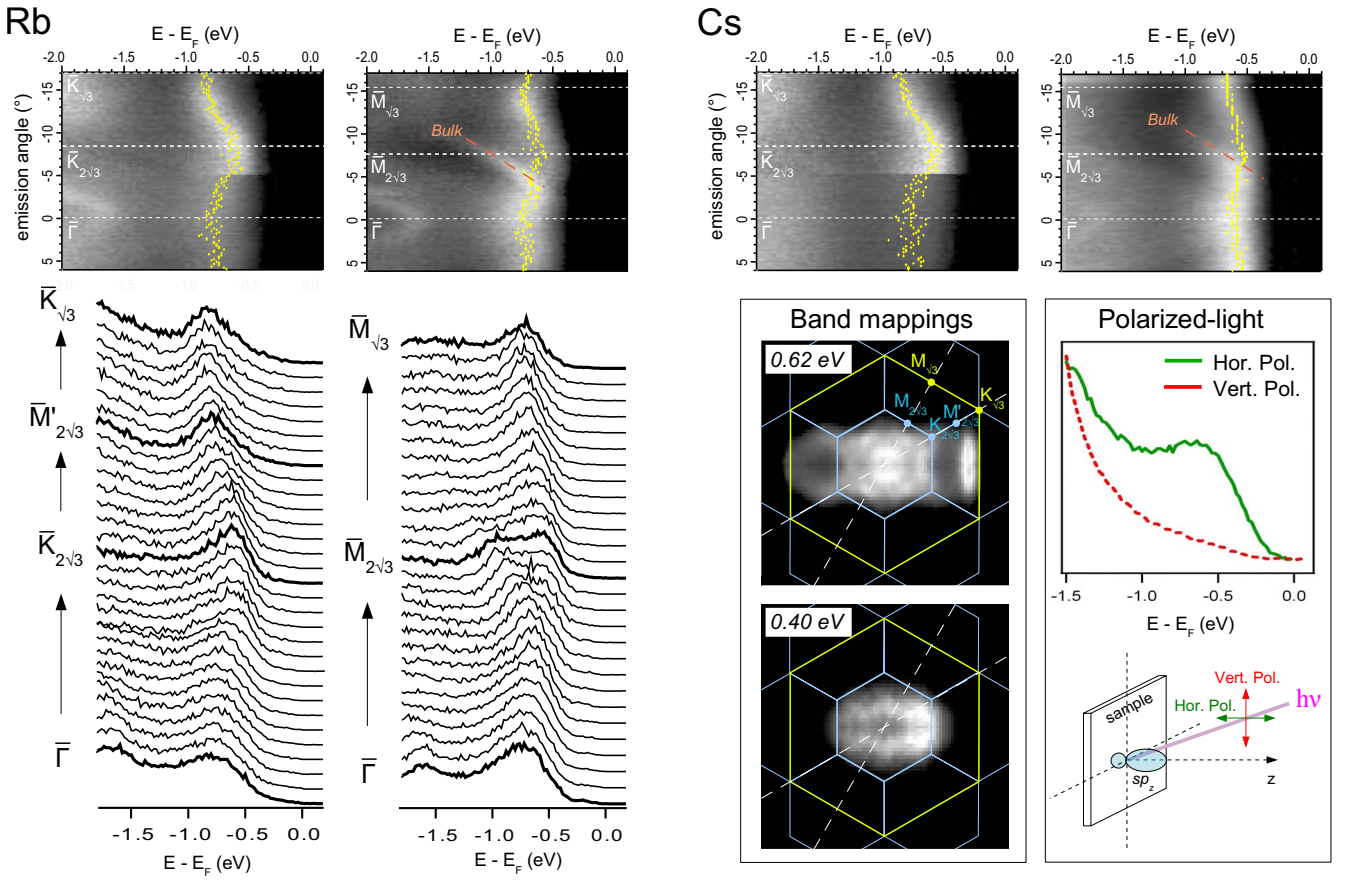

FIG. 4. (Color online) Electronic band structure of the Rb and Cs/Si:B-$2\sqrt{3}$ interfaces at low (55 K) temperature. Top: photoemission $I(E,\theta)$ intensity maps, for the $\bar{\Gamma}\bar{K}_{\sqrt{3}}$ and $\bar{\Gamma}\bar{M}_{\sqrt{3}}$ directions of the Brillouin zone. First, a weaker dispersion is observed in the $\bar{\Gamma}\bar{M}_{\sqrt{3}}$ direction; second, the surface-state band has an extremum at the edge of the $2\sqrt{3}$ Brillouin zone. Bottom, left: selection of EDCs for the Rb interface, extracted from the above intensity maps. Bottom, right: for Cs, two band mappings taken at different binding energies are plotted (see text for details). Finally, polarized-light measurements (see scheme) confirm the Cs surface-state sp_z symmetry.

mechanism); in particular, at the $\bar{M}'_{2\sqrt{3}}$ point, there *must* be a band folding. In the present work, the discrepancy concerning the surface-state symmetry is solved: a careful inspection of the ARPES spectra show that *two* subbands—labeled by "+" and "−"—having the correct, $2\sqrt{3}$ symmetry constitute what we called previously "the" surface state. In the present case, the two-band surface-state analysis is carried out for the Rb/Si:B-$2\sqrt{3}$ interface at 55 K, Fig. 5, with special focus on EDCs taken along the $\bar{K}_{2\sqrt{3}}\rightarrow\bar{M}'_{2\sqrt{3}}\rightarrow\bar{K}_{\sqrt{3}}$ segment (see band mappings, Fig. 4). The EDCs line shape is reproduced by the sum of two Gaussian functions (the plain and dotted lines refer to the + and − subbands, respectively). At the $\bar{K}_{2\sqrt{3}}$ and $\bar{K}_{\sqrt{3}}$ points, the energy of each subband is kept constant ($E^+=-0.58$ eV and $E^-=-0.86$ eV). In addition at these points, we can determine the linewidth of each subband ($\Gamma^+=0.34$ eV and $\Gamma^-=0.40$ eV) with accuracy because one contribution is dominant. Between $\bar{K}_{2\sqrt{3}}$ and $\bar{K}_{\sqrt{3}}$, the spectral weight and the binding energy of each contribution is allowed to vary, but the linewidth is kept constant. The + and − subbands have important spectral weight in the $\bar{K}_{2\sqrt{3}}\rightarrow\bar{M}'_{2\sqrt{3}}$ and $\bar{M}'_{2\sqrt{3}}\rightarrow\bar{K}_{\sqrt{3}}$ segments, respectively. When going from $\bar{K}_{2\sqrt{3}}$ to $\bar{K}_{\sqrt{3}}$, the spectral weight is transferred progressively from the + to the − subband. At $\bar{M}'_{2\sqrt{3}}$, the two subbands have same weight; in addition, the $2\sqrt{3}$ symmetry forces a band folding with an energy gap opening: experimentally, we determine this gap is about 0.2 eV. Note the amplitude of the subbands dispersion is extremely small (only 50 meV). Unlike the energy eigenvalues, the spectral weight of the two subbands is thus not periodic in the reciprocal space;[54] this explains our previous, erroneous analysis.[14,53] Lastly, let us discuss the total number of bands one should observe with ARPES. A $2\sqrt{3}$ unit cell contains four Si adatoms so *four* bands must arise from the unperturbated dangling-bond surface state. With a 1/2 ML saturation coverage and assuming all *ns* electrons are transferred to the dangling bonds, each $2\sqrt{3}$ unit cell contains six electrons. Thus *three* bands should be filled; we observe two of them but have no clear evidence for the last third. It is possible that the lacking band is blended with the two subbands. The fourth, unoccupied band may be related to the "S_2" state, observed by Weitering *et al.* with inverse photoemission.[15]

In Fig. 6, we compare the surface-state dispersion for the different alkali's. For this, we compare EDCs taken at the $\bar{K}_{2\sqrt{3}}$ (thick lines) and $\bar{K}_{\sqrt{3}}$ (thin lines) points on K, Rb, and Cs pure interfaces. Room (left panel) and low (55 K, right panel) temperatures have been considered. From these EDCs

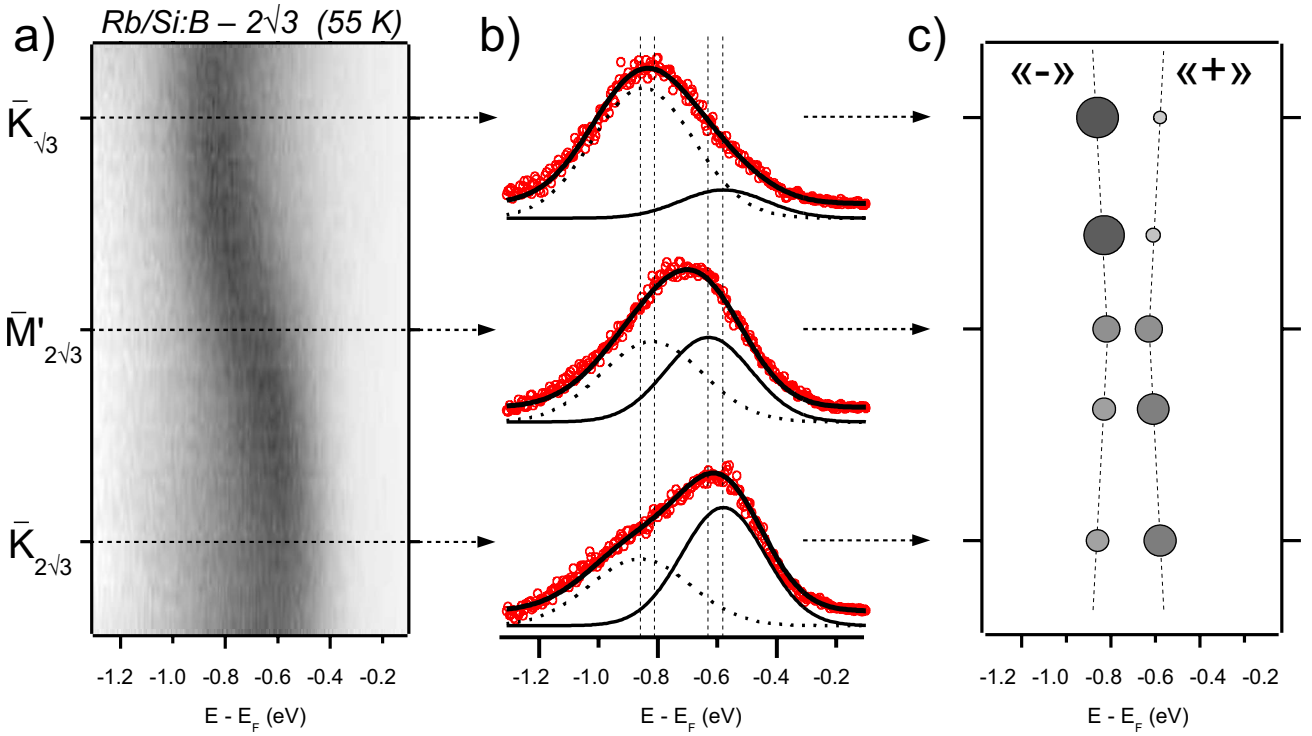

FIG. 5. (Color online) Two-band surface-state analysis. Sample is Rb/Si:B-$2\sqrt{3}$ at 55 K. (a) ARPES intensity map focusing on the $\bar{K}_{2\sqrt{3}} \rightarrow \bar{M}'_{2\sqrt{3}} \rightarrow \bar{K}_{\sqrt{3}}$ segment. (b) Deconvolution of the EDCs with two Gaussian functions; see text for details. (c) Dispersions (dashed lines) and spectral weights (filled circles, which radius and darkness increase as the spectral weight) of the + and − subbands, extracted from the fits. They are very weakly dispersive ($\approx$50 meV) and separated by a 0.2 eV gap at the $\bar{M}_{2\sqrt{3}}$ point.

we determine the binding energy E_B^+ of the so-called + surface-state subband. We define it as the maximum of the state dispersion, that is $E_B^+ \equiv E^+(\bar{K}_{2\sqrt{3}})$; it is indicated by the dotted vertical line. According to Fig. 5, the surface-state bandwidth is integrated over the two subbands; thus we have $W \equiv E^-(\bar{K}_{\sqrt{3}}) - E^+(\bar{K}_{2\sqrt{3}})$. Let us discuss first the binding energy. At room temperature, E_B^+ is higher for K, and it is roughly the same for Rb and Cs interfaces. At 55 K, the surface state shifts systematically toward higher binding energies. However the shift amplitude depends on the alkali: it is rather weak (50 meV) for Rb and Cs, but more pronounced for K (120 meV). K still exhibits the highest binding energy at low temperature, and a closer inspection with better statistics shows that Cs has actually a binding energy 30 meV smaller than Rb (see bottom of Fig. 6). Concerning bandwidth, at room temperature, W is 0.22, 0.26, and 0.28 eV for K, Rb, and Cs, respectively. At 55 K, the bandwidth remains the same for the three alkali's. Since the experimental energy increment is 20 meV for these measurements, we can conclude that K has the smallest bandwidth but cannot distinguish between Rb and Cs.

In order to confirm that the band features evolve systematically when moving across the alkali column, we present ARPES data (300 K) concerning the $K_{0.4}Rb_{0.6}$ alloy (Fig. 7). This choice of alloy is motivated by the fact it has been possible to observe clear differences between K and Rb surface states (Fig. 6). On the left panel, the series of EDCs taken along the $\bar{\Gamma}\bar{K}$ direction exhibits the typical band extremum at the $\bar{K}_{2\sqrt{3}}$ found in the pure K and Rb interfaces. On the right panel, we compare the EDCs taken at high-symmetry points for the alloy (plain lines) and the pure interfaces (pink dotted and red dashed lines are for K and Rb, respectively). First, the line broadening of the alloy surface state is very similar to pure interfaces meaning that no significant disorder is induced when forming the alloy; this corroborates the LEED observation [Fig. 3(a)]. Second, the alloy surface state is located half way between the K and Rb surface states, as shown at the $\bar{K}_{2\sqrt{3}}$, $\bar{M}'_{2\sqrt{3}}$, and $\bar{K}_{\sqrt{3}}$ points. From this observation, we can conclude fairly that the surface-state binding energy is changed *continuously* in the alkali series.

To finish with the electronic properties of the alkali/Si:B-$2\sqrt{3}$ interfaces, we have studied the temperature effect on the surface-state linewidth (energy broadening). In the following we note Γ the full-width at half maximum. In a general way, broadening may arise from experimental resolution but mainly from disorder and many-body processes.[33] In our case, the spectral structures are so broad that experimental contribution is completely negligible. In Fig. 8 (left panel), EDCs taken at the $\bar{K}_{2\sqrt{3}}$ point at room (plain red line) and low (55 K, dotted blue line) temperatures for each alkali are compared. On these graphs, we have set $E_B^+ = 0$ for all alkali's. At room temperature, $\Gamma/2 \approx 0.2$ eV for K, Rb, and Cs. For Rb and Cs, a clear narrowing ($\Gamma/2 \approx 0.12$ eV) is observed upon cooling the sample to 55 K; this effect is much weaker with K. In the right panel, same spectra (for K and Cs) are plotted differently to enhance the alkali substitution effect.

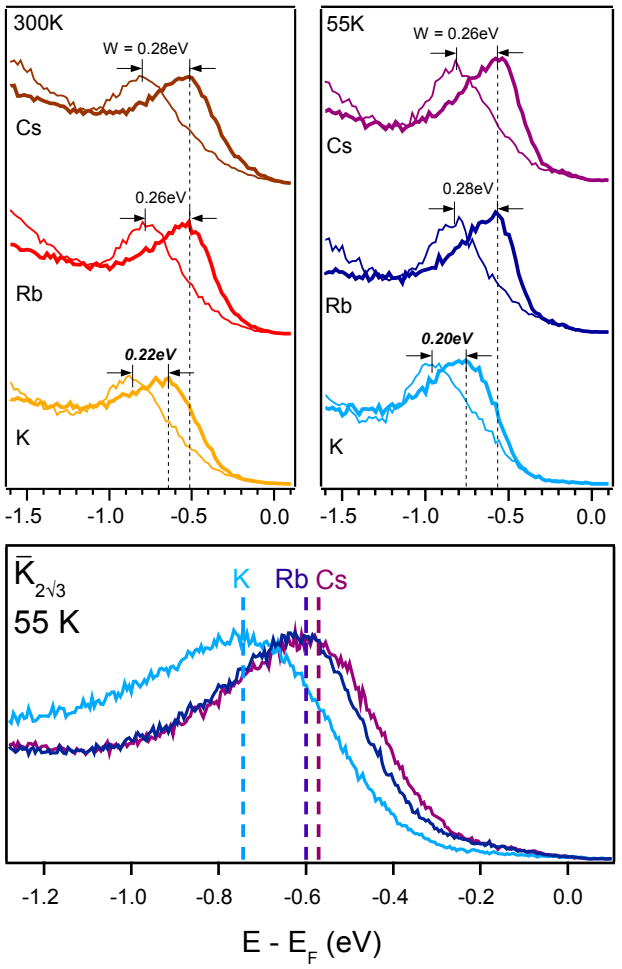

FIG. 6. (Color online) Surface-state dispersion analysis at 300 and 55 K. Top: the thick and thin lines are EDCs taken at the $\bar{K}_{2\sqrt{3}}$ and $\bar{K}_{\sqrt{3}}$ points. The vertical dashed lines indicates E_B^+, the maximum of the + subband dispersion. A smaller bandwidth is observed with K whereas it is the same for both Rb and Cs interfaces. At low temperature, the surface state shifts systematically toward high binding energies; the effect is more pronounced for K. Bottom: ARPES spectra taken on same samples with better statistics show that the Cs surface state has actually a smaller binding energy.

Let us summarize the main results of this section: (i) whatever the alkali, the electronic structure of the alkali/Si:B-$2\sqrt{3}$ interfaces is characterized by a *two-band* surface state, which is *insulating*, *weakly dispersive* and *very broad*, (ii) as substituting the alkali from K to Cs, the binding energy reduces while the bandwidth increases, and (iii) upon cooling, a systematic *shift* of the surface state toward higher binding energies is observed together with a *narrowing* of the ARPES line; we have shown that the largest shift and smallest narrowing are found with K. All numerical values can be found in Table I.

B. Spectral function analysis in the bipolaron model

This *bipolaron* model[37,38] has been proposed by us to describe the physics of the K/Si:B-$2\sqrt{3}$ interface.[14] Before discussing the results in the framework of this model, just recall

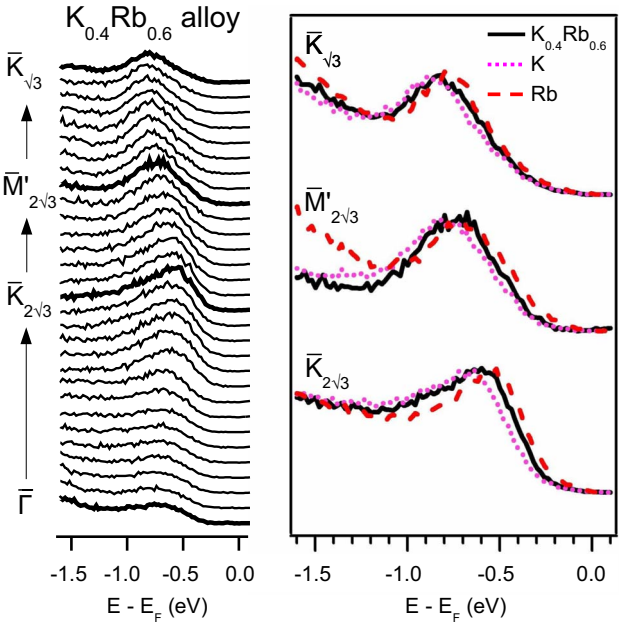

FIG. 7. (Color online) Electronic band structure of the $K_{0.4}Rb_{0.6}$-$2\sqrt{3}$ solid solution at room temperature. The dispersion of the surface state is sandwiched between those of the pure K and Rb interfaces. The linewidth is similar to pure interfaces, indicating a homogeneous solid solution instead of K and Rb domains.

the former interpretation—the Mott insulating ground state—proposed by Weitering *et al.*[15,16] Assuming saturation coverage to be $\frac{1}{3}$ ML, alkali atoms provide one electron per each $\sqrt{3}$ unit cell leading to a half-filled sp_z surface band.[55] However, ARPES indicates clearly a fully occupied state. The Harrison criterion[7] for Mott insulating ground state ($\frac{U}{W}$

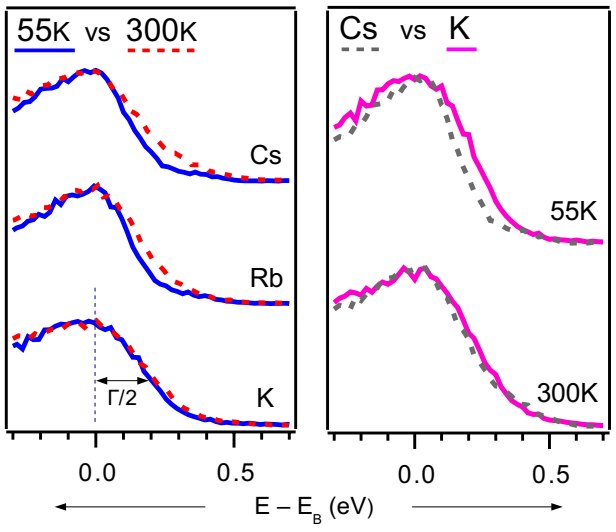

FIG. 8. (Color online) Surface-state linewidth analysis at low (55 K) and room temperatures. Left panel: the plain blue and dotted red lines refer to low and room temperature, respectively. Right panel: the plain and dotted lines refer to K and Cs/Si:B-$2\sqrt{3}$ interfaces, respectively. For K, the ARPES line broadens slightly when increasing temperature whereas for Rb and Cs the effect is more pronounced.

TABLE I. Experimental binding energies (E_B^+), bandwidth (W), and half-width at half maximum ($\frac{\Gamma}{2}$) for K, Rb, and Cs/Si:B-$2\sqrt{3}$ surface state at 55 K. Values in italics refer to room-temperature measurements.

	E_B^+ (eV)	W (eV)	$\frac{\Gamma}{2}$ (eV)
K	0.75 (*0.64*)	0.20 (*0.22*)	0.18 (*0.20*)
Rb	0.60 (*0.52*)	0.28 (*0.26*)	0.12 (*0.18*)
Cs	0.57 (*0.52*)	0.26 (*0.28*)	0.12 (*0.20*)

≥ 2) was estimated using the experimental bandwidth $W \approx 0.2$ eV and a typical on-site repulsion $U=1-2$ eV and found to be strongly satisfied on this surface.[15] The very broad ARPES line, attributed to strong electron-phonon interaction, was already emphasized and the bipolaronic ground state was even suggested. It was discarded, however, because no doubling of the unit cell was observed in LEED.

From a theoretical point of view, the simplest way to tackle both strong electron-electron and electron-phonon interactions is to consider the Holstein-Hubbard (HH) model (for a review, see Ref. 56). A fundamental parameter which emerges from it is the *effective* on-site repulsion $U_{eff} \equiv U - 2g^2\hbar\omega_0$, where g is the electron-phonon coupling constant and $\hbar\omega_0$ is the typical phonon energy. The reason why electron repulsion U is renormalized into U_{eff} is that carriers are *polarons*, that is electrons which are self-trapped in a lattice deformation; when two polarons encounter, in addition to the Coulomb repulsion, each feels the *attractive* potential of the other one. At half-filling, the Mott insulator is the ground state if U_{eff} remains positive. If $U_{eff}<0$, however, polaronic effects dominate electron repulsion so that electrons can bind into localized pairs associated with a lattice distortion: the *bipolarons*. At half filling on the one-dimensional (1D) chain, the corresponding ground state is the so-called *bipolaronic* insulator,[38] which can be visualized as an enhanced Peierls CDW (Refs. 57 and 58) (see top of Fig. 9). The set of results reported in this paper for both structural (the $2\sqrt{3}$ reconstruction) and electronic (the gap, the band-folding and the broad line) properties, common to all alkali/S:B interfaces, are consistent with the bipolaronic ground state. In Fig. 9 (bottom), we propose a simple charge-ordering pattern for the alkali/Si:B-$2\sqrt{3}$ interfaces. There are four Si adatoms (blue bowls), and then four empty sp_z dangling bonds per $2\sqrt{3}$ unit cell. Moreover, our determination of the absolute coverage[42] indicates six alkali atoms (not represented in the figure) in the same cell. Assuming the six ns electrons are transferred to the dangling bonds, we can form three doubly occupied sites (the bipolarons) and one empty site.

ARPES measures basically the one-electron spectral function $A(\vec{k},E)$ in the occupied part of the excitation spectrum.[33] When electron-phonon coupling is strong, the HH spectral function is approximated by the Lang-Firsov expression (zero-bandwidth limit).[59,60] In this case, there is no $\vec{k}$ dependency. For $U_{eff}<0$, i.e., the bipolaronic insulator, the spectral function consists in two broad Frank-Condon polaronic structures separated by a total gap $2\Delta=-U_{eff}+2g^2\hbar\omega$ with the Fermi level midgap[34,53,61] (see Fig. 10). For very strong

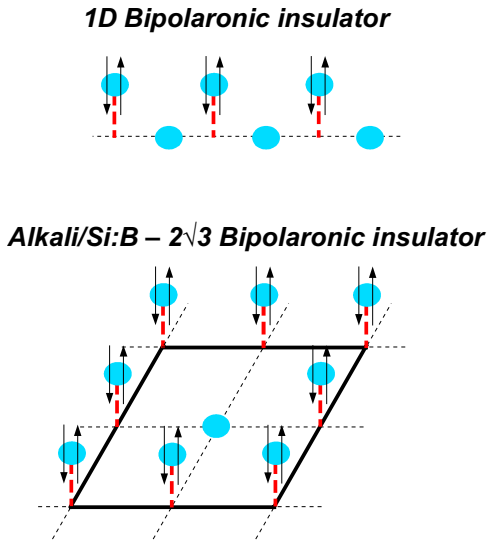

FIG. 9. (Color online) The bipolaronic insulator. Top: sketch of charge ordering and lattice distortion in the 1D bipolaronic insulator at half filling. Bottom: bipolaron charge-ordering pattern proposed for alkali/Si:B-$2\sqrt{3}$; the thick black line indicates the $2\sqrt{3}$ unit cell. There are six electrons per unit cell; equivalently, the dangling bond is 3/4 filled.

coupling, these *incoherent* structures tend to Gaussian functions. The zero-phonon peaks—the *quasiparticle* states—are separated by $-U_{eff}$ and show very weak spectral intensity because coupling is very strong. In Fig. 11, the experimental ARPES spectra presented in Fig. 8 are analyzed within this theoretical result. The EDC is chosen at the extremum of the band ($\bar{K}_{2\sqrt{3}}$ point) because this is where the CDW gap is defined usually.[58] A Shirley background has been removed (see insets); by doing so, we recover a symmetrical spectral feature related to the +, dominant state (see Fig. 5). We assume the typical phonon to be the vibration of the surface Si tetrahedron; its energy is $\hbar\omega_0=55$ meV according to electron-energy-loss measurements[40,62] performed on the Si:B substrate.

First examine the room-temperature data for both K and Cs/Si:B-$2\sqrt{3}$ interfaces (red lines). This choice is motivated by the fact that Cs and K exhibit the weakest and strongest polaronic effects, respectively. Although not shown here, Rb would give very similar results as for Cs. For K, the best fit

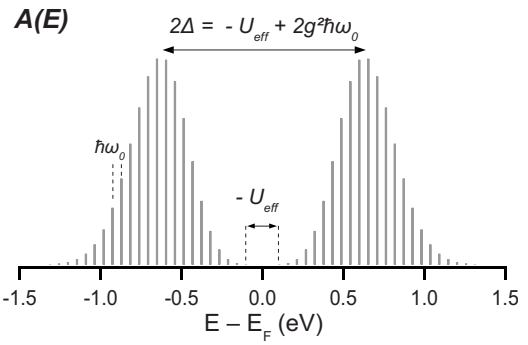

FIG. 10. One-electron spectral function $A(E)$ for negative U_{eff}, in the zero-bandwidth Holstein-Hubbard model.

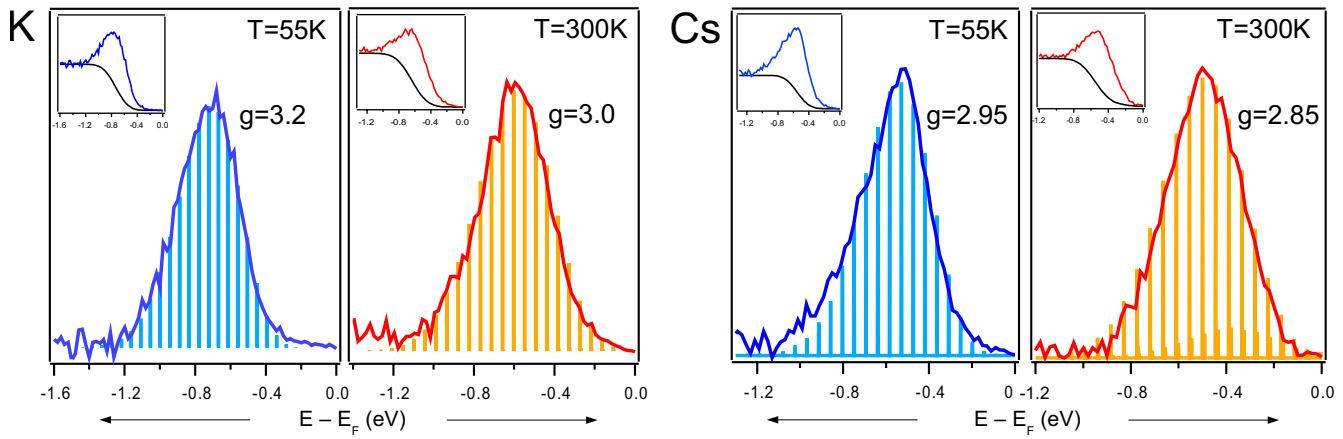

FIG. 11. (Color online) Spectral function simulation of the K and Cs/Si:B-$2\sqrt{3}\times 2\sqrt{3}R30°$ surface state at low (55 K) and room temperatures. The typical phonon energy is $\hbar\omega$=55 meV, according to Refs. 40 and 62. The deduced Hubbard term is U=0.78 eV for *both* alkali and temperatures. We emphasize here that by decreasing the e-ph coupling constant when increasing temperature, it is possible to reproduce the energy shift of the surface state. Insets: substraction of a Shirley background from the raw data.

(red vertical bars) which reproduces both the ARPES linewidth and maximum intensity position is obtained with g =3.0 and U=0.78 eV; this corresponds to a very strong electron-phonon coupling and to a negative effective Hubbard term U_{eff}=−0.35 eV. With the same U and $\hbar\omega_0$, we found that a lower value g=2.85 is necessary to fit well the Cs interface; this gives U_{eff}=−0.11 eV. Thus the Cs/Si:B interface is close to *metallization* (that is, U_{eff}=0), as already suggested by Weitering *et al.*[15] in their analysis of electron-energy-loss spectra.[63] In addition, this is consistent with the systematic observation of a less sharp $2\sqrt{3}$ LEED pattern with Cs (Fig. 2). Concerning temperature effects, this explains probably why a stronger linewidth variation with temperature is observed experimentally for Cs (Fig. 8). Indeed in the polaron theory, one shows[61] that the width of the Frank-Condon incoherent structures is $\Gamma \approx g\hbar\omega_0\sqrt{\frac{1}{2}\coth(\frac{\hbar\omega_0}{2kT})}$ in the strong-coupling limit. In addition, the larger g may be responsible for the smaller bandwidth observed on K/Si:B (Table I), since the polaron bandwidth is renormalized[56] as e^{-g^2}. We do not have simple explanation why g is higher in K; naively, this is even unexpected since for alkali halides (the prototypical polaronic materials) the contrary occurs.[52] On the other hand, the same is observed on the much more similar alkali/GaAs(110) interfaces.[35,36] Polaronic effects are reduced with increasing alkali atomic number while the Hubbard term U does not depend on the adsorbate,[35] as in our assumption. The values of U_{eff} are −0.61 eV and −0.35 eV for Na and K, respectively; in the case of Cs, electron-energy-loss measurements[64] suggest that the weakening of the electron-phonon coupling even allows U_{eff} to become positive, leading to the Mott state. Although not considered here, another way to reduce the gap is assuming that the phonon energy lowers from K to Cs.

Now turn to the low-temperature measurements (55 K, blue line). Two systematic effects have been noticed in the previous section: (i) the narrowing of the ARPES line and (ii) a shift of the surface state toward higher binding energies. If we use the same fitting parameters as before, the narrowing of the spectral function is not well reproduced. In both cases, it is necessary to increase the electron-phonon coupling constant (3.0→3.2 and 2.85→2.95 for K and Cs, respectively). Although surprising, this has been evidenced already on heavily doped diamond samples,[65] in which hole careers are strongly coupled ($g \approx 1.2$) to a 150 meV optical phonon. It is reasonable to assume that this property should be extended to Si:B since both are degenerate (metallic) semiconductors. Interestingly for our purpose, this leads to a shift of the Frank-Condon structure toward higher binding energies when decreasing temperature (we recall that its position with respect to the Fermi level is $\Delta = 2g^2\hbar\omega_0 - \frac{U}{2}$). These values of g give an energy shift of 135 and 65 meV for K and Cs, in good agreement with the 110 and 50 meV values given by direct measurement (Table I). In conclusion, the bipolaron model gives a consistent explanation for the observed temperature effects, which magnitude depends on the alkali. Our analysis shows that K exhibits stronger polaronic effects than Cs, as already demonstrated on similar alkali/semiconductor interfaces.

V. CONCLUSION

In conclusion, we have presented a systematic study of the alkali/Si:B interfaces, including solid solution, in order to confirm previous results concerning K. By combining LEED, XPS, and ARPES, we show that physics are basically the same for all interfaces at saturation coverage. The $2\sqrt{3}$ symmetry is found to be a common property, for both structural and electronic properties. From a theoretical point of view, the spectral function of the insulating surface state is analyzed within the bipolaron model, which is appropriate for systems with strong electron-phonon coupling. This allows

to reproduce the systematic, fine temperature effects observed on the linewidth and binding energy; K is shown to exhibit stronger polaronic effects than Rb and Cs. Finally, a new 3×3 reconstruction is evidenced for a coverage that is possibly 1/3 ML; it would be interesting to know whether or not this phase is common to that observed on Sn/Ge.

ACKNOWLEDGMENTS

The authors would like to thank L. Moreau for his technical support (especially for the design of the alkali evaporator), W. Srour and M. Stoffel for their contribution to the experiments, and E.G. Michel for fruitful discussions.

*tournier@lpm.u-nancy.fr

[1] A. Zangwill, *Physics at Surfaces* (Cambridge University Press, Cambridge, 1988).

[2] M. Berthe, A. Urbieta, L. Perdigão, B. Grandidier, D. Deresmes, C. Delerue, D. Stiévenard, R. Rurali, N. Lorente, L. Magaud, and P. Ordejón, Phys. Rev. Lett. **97**, 206801 (2006).

[3] E. Tosatti and P. W. Anderson, J. Appl. Phys. **2**, 2381 (1974).

[4] G. Santoro, S. Scandolo, and E. Tosatti, Phys. Rev. B **59**, 1891 (1999).

[5] N. F. Mott, Proc. R. Soc. London, Ser. A **62**, 416 (1949).

[6] J. Hubbard, Proc. R. Soc. London, Ser. A **276**, 238 (1963); **277**, 237 (1964); **281**, 401 (1964).

[7] W. A. Harrison, Phys. Rev. B **31**, 2121 (1985).

[8] F. Gebhard, *Mott Metal-Insulator Transition: Models and Methods*, Springer Tracts in Modern Physics (Springer, Berlin, 1997).

[9] Y. Ma, J. E. Rowe, E. E. Chaban, C. T. Chen, R. L. Headrick, G. M. Meigs, S. Modesti, and F. Sette, Phys. Rev. Lett. **65**, 2173 (1990).

[10] H. J. W. Zandvliet, H. B. Elswijk, E. J. van Loenen, and D. Dijkkamp, Phys. Rev. B **45**, 5965 (1992).

[11] T. M. Grehk, L. S. O. Johansson, U. O. Karlsson, and A. S. Flodström, Phys. Rev. B **47**, 13887 (1993).

[12] H. H. Weitering, J. Chen, N. J. DiNardo, and E. W. Plummer, Phys. Rev. B **48**, 8119 (1993).

[13] T. M. Grehk, M. Göthelid, U. O. Karlsson, L. S. O. Johannson, S. M. Gray, and K. O. Magnusson, Phys. Rev. B **52**, 11165 (1995).

[14] L. A. Cardenas, Y. Fagot-Revurat, L. Moreau, B. Kierren, and D. Malterre, Phys. Rev. Lett. **103**, 046804 (2009).

[15] H. H. Weitering, X. Shi, P. D. Johnson, J. Chen, N. J. DiNardo, and K. Kempa, Phys. Rev. Lett. **78**, 1331 (1997).

[16] C. S. Hellberg and S. C. Erwin, Phys. Rev. Lett. **83**, 1003 (1999).

[17] J. M. Carpinelli, H. H. Weitering, E. W. Plummer, and R. Stumpf, Nature (London) **381**, 398 (1996).

[18] J. M. Carpinelli, H. H. Weitering, M. Bartkowiak, R. Stumpf, and E. W. Plummer, Phys. Rev. Lett. **79**, 2859 (1997).

[19] R. I. G. Uhrberg and T. Balasubramanian, Phys. Rev. Lett. **81**, 2108 (1998).

[20] J. Avila, A. Mascaraque, E. G. Michel, M. C. Asensio, G. LeLay, J. Ortega, R. Pérez, and F. Flores, Phys. Rev. Lett. **82**, 442 (1999).

[21] F. Flores, J. Ortega, R. Pérez, A. Charrier, F. Thibaudau, J.-M. Debever, and J.-M. Themlin, Prog. Surf. Sci. **67**, 299 (2001).

[22] R. Cortés, A. Tejeda, J. Lobo, C. Didiot, B. Kierren, D. Malterre, E. G. Michel, and A. Mascaraque, Phys. Rev. Lett. **96**, 126103 (2006).

[23] G. Profeta and E. Tosatti, Phys. Rev. Lett. **98**, 086401 (2007).

[24] A. Tejeda, R. Cortés, J. Lobo-Checa, C. Didiot, B. Kierren, D. Malterre, E. G. Michel, and A. Mascaraque, J. Phys.: Condens. Matter **19**, 355008 (2007).

[25] A. Tejeda, R. Cortés, J. Lobo-Checa, C. Didiot, B. Kierren, D. Malterre, E. G. Michel, and A. Mascaraque, Phys. Rev. Lett. **100**, 026103 (2008).

[26] R. I. G. Uhrberg, H. M. Zhang, T. Balasubramanian, S. T. Jemander, N. Lin, and G. V. Hansson, Phys. Rev. B **62**, 8082 (2000).

[27] J. Lobo, A. Tejeda, A. Mugarza, and E. G. Michel, Phys. Rev. B **68**, 235332 (2003).

[28] S. Modesti, L. Petaccia, G. Ceballos, I. Vobornik, G. Panaccione, G. Rossi, L. Ottaviano, R. Larciprete, S. Lizzit, and A. Goldoni, Phys. Rev. Lett. **98**, 126401 (2007).

[29] L. I. Johansson, F. Owman, and P. Martensson, Surf. Sci. **360**, L478 (1996).

[30] J.-M. Themlin, I. Forbeaux, V. Langlais, H. Belkhir, and J.-M. Debever, Europhys. Lett. **39**, 61 (1997).

[31] J. E. Northrup and J. Neugebauer, Phys. Rev. B **57**, R4230 (1998).

[32] V. Ramachandran and R. M. Feenstra, Phys. Rev. Lett. **82**, 1000 (1999).

[33] S. Hüfner, *Photoemission Spectroscopy: Principles and Application*, 3rd ed. (Springer, New York, 2003).

[34] G. D. Mahan, *Many-Particle Physics* (Plenum Press, New York, 1990).

[35] O. Pankratov and M. Scheffler, Phys. Rev. Lett. **71**, 2797 (1993).

[36] U. del Pennino, B. Salvarani, R. Compano, and O. Pankratov, Phys. Rev. B **52**, 10717 (1995).

[37] A. S. Alexandrov and N. F. Mott, *Polarons and Bipolarons* (World Scientific, Singapore, 1996).

[38] U. Göbel, A. S. Alexandrov, and H. Capellmann, Z. Phys. B: Condens. Matter **96**, 47 (1994).

[39] P. Dai, Y. Zhang, and M. P. Sarachik, Phys. Rev. Lett. **66**, 1914 (1991).

[40] J. E. Rowe, R. A. Malic, E. E. Chaban, R. L. Headrick, and L. C. Feldman, J. Electron Spectrosc. Relat. Phenom. **54-55**, 1115 (1990).

[41] P. J. Chen, J. E. Rowe, and J. T. Yates, Phys. Rev. B **50**, 18134 (1994).

[42] C. Tournier-Colletta *et al.* (unpublished).

[43] See beamline website: http://www.synchrotron-soleil.fr/Recherche/LignesLumiere/CASSIOPEE, for information.

[44] M. Sprinkle, D. Siegel, Y. Hu, J. Hicks, A. Tejeda, A. Taleb-Ibrahimi, P. Le Fèvre, F. Bertran, S. Vizzini, H. Enriquez, S. Chiang, P. Soukiassian, C. Berger, W. A. de Heer, A. Lanzara, and E. H. Conrad, Phys. Rev. Lett. **103**, 226803 (2009).

[45] K. Sakamoto and R. I. G. Uhrberg, e-J. Surf. Sci. Nanotechnol. **2**, 210 (2004).

[46] F. Amy and P. Soukiassian, Appl. Phys. Lett. **85**, 926 (2004).
[47] C. Törnevik, M. Hammar, N. G. Nilsson, and S. A. Flodström, Phys. Rev. B **44**, 13144 (1991).
[48] P. E. J. Eriksson, J. R. Osiecki, K. Sakamoto, and R. I. G. Uhrberg, Phys. Rev. B **81**, 235410 (2010).
[49] P. A. Lee, T. M. Rice, and P. W. Anderson, Phys. Rev. Lett. **31**, 462 (1973).
[50] L. J. Sham and B. R. Patton, Phys. Rev. B **13**, 3151 (1976).
[51] J. A. R. Stiles, D. L. Williams, and M. J. Zuckermann, J. Phys. C **9**, L489 (1976).
[52] C. Kittel, *Quantum Theory of Solids* (Wiley, New York, 1987).
[53] C. Tournier-Colletta, L. Cardenas, Y. Fagot-Revurat, B. Kierren, and D. Malterre, J. Electron Spectrosc. Relat. Phenom. **181**, 76 (2010).
[54] C. Didiot, Y. Fagot-Revurat, S. Pons, B. Kierren, C. Chatelain, and D. Malterre, Phys. Rev. B **74**, 081404 (2006).
[55] H. Q. Shi, M. W. Radny, and P. V. Smith, Phys. Rev. B **70**, 235325 (2004).
[56] J. T. Devreese and A. S. Alexandrov, Rep. Prog. Phys. **72**, 066501 (2009).
[57] R. E. Peierls, *Quantum Theory of Solids* (Oxford University Press, New York, 1955).
[58] G. Grüner, Rev. Mod. Phys. **60**, 1129 (1988).
[59] I. G. Lang and Y. A. Firsov, Sov. Phys. JETP **16**, 1301 (1963).
[60] M. Berciu, Phys. Rev. Lett. **97**, 036402 (2006).
[61] R. A. Bari, Phys. Rev. B **9**, 4329 (1974).
[62] M. Fontaine and J.-M. Layet, J. Electron Spectrosc. Relat. Phenom. **64-65**, 201 (1993).
[63] H. H. Weitering, J. Chen, R. Pérez-Sandoz, and N. J. DiNardo, Surf. Sci. **307-309**, 978 (1994).
[64] N. J. DiNardo, T. M. Wong, and E. W. Plummer, Phys. Rev. Lett. **65**, 2177 (1990).
[65] K. Ishizaka, R. Eguchi, S. Tsuda, A. Chainani, T. Yokoya, T. Kiss, T. Shimojima, T. Togashi, S. Watanabe, C.-T. Chen, Y. Takano, M. Nagao, I. Sakaguchi, T. Takenouchi, H. Kawarada, and S. Shin, Phys. Rev. Lett. **100**, 166402 (2008).